Article citation info:
Wróblewski P, Bratkowski P, Kachel S. Investigation of the influence of propeller blade profile and angle of attack on the performance parameters of an aircraft piston engine. Combustion Engines. 2026;204(1):119-131. https://doi.org/10.19206/CE-208772

Piotr WRÓBLEWSKI
Przemysław BRATKOWSKI
Stanisław KACHEL

Combustion Engines
Polish Scientific Society of Combustion Engines

Investigation of the influence of propeller blade profile and angle of attack on the performance parameters of an aircraft piston engine

ARTICLE INFO

Received: 3 April 2025
Revised: 23 July 2025
Accepted: 29 July 2025
Available online: 22 September 2025

This article presents the results of experimental research concerning the influence of propeller blade profile and angle of attack on the performance parameters of the 3W 275 XI B2 CS aircraft piston engine. A specialised test stand was utilised, enabling real-time measurement of thrust, cylinder head temperature, and crankshaft rotational speed. The research was conducted with various propeller configurations (2- and 3-bladed) and at differing rotational speeds, which allowed for an assessment of the impact of propeller geometry on engine operational efficiency. The findings demonstrated that appropriate selection of the angle of attack, blade profile, and number of blades significantly affects the achieved parameters – particularly thrust and temperature distribution, which is of critical importance for the safety and durability of the powertrain components. The developed test stand facilitates further research into propeller selection for light aircraft piston combustion engines.

A novel aspect of this work is the utilisation of a new type of test stand that permits the determination of changes in thrust values obtained during tests across wide ranges of engine crankshaft rotational speeds. The selection of propellers, considering the number of blades and their profile, is very difficult to predict and should always be undertaken individually for each engine following testing. Such a tailored blade profile and number of propeller blades allow for high engine operational flexibility and good propeller thrust depending on the crankshaft's rotational speed.

Key words: *propeller blade profile, angle of attack, thrust, bench tests, two-stroke aircraft engine*

1. Introduction

Contemporary ultralight aviation and the unmanned aerial vehicle (UAV) sector are undergoing rapid development. This, in turn, translates into an increasing market demand for economical and highly reliable piston combustion engines. This is particularly pertinent in the domain of two-stroke engines, which, owing to their design and low inherent mass, are gaining popularity among light aircraft designers. From the perspective of enhancing thrust and reducing fuel consumption, a critical factor influencing the development of these engines is the appropriate selection of propeller geometry. This primarily involves the selection of the blade profile and angle of attack. The interaction between the propeller design and the piston combustion engine significantly impacts the thrust generated, the efficiency of the propulsion system, and the engine's thermal and mechanical parameters. The correct selection of blade shape and angle of attack can lead not only to increased thrust and fuel savings but also to improved cooling and more uniform load distribution. From the standpoint of flight safety and the durability of the piston combustion engine, several factors are of particular importance: cooling the engine cylinder heads, ensuring adequate lubrication at high temperatures, and defining the engine's cooling range for selected propeller parameters. It is important to note that two-stroke engines designed to power small aircraft are cooled exclusively by ambient air. An additional cooling airflow is generated by the propeller's thrust, as it is typically positioned directly adjacent to the engine. This arrangement ensures the appropriate shaping of the air stream, which is dependent on both the propeller geometry and the aircraft's cruising speed. Furthermore, it must also be considered that the direct coupling of the propeller to the engine's crankshaft imposes additional stresses on the engine's primary mechanical components, in the form of complex vibrations transmitted to the engine block.

In the case of small aircraft – both manned and unmanned aerial vehicles (UAVs) – the propeller remains a key element of the propulsion system [15]. It is responsible for the amount of thrust generated, which is why its design and its matching to a specific engine, most often a piston type, have a significant impact on performance, fuel consumption, and the overall reliability of the drive system [15]. Low-power piston engines – in the range of a few to several dozen horsepower – are widely used in unmanned aerial vehicles, models, and manned light aviation [7]. They typically work in conjunction with two- or three-bladed propellers made from wood, metal, or composites [7]. A conceptual design for the construction of an unmanned aerial vehicle was also presented in [9], which primarily described the design assumptions and concepts for the propulsion system [9].

The propeller, as a rotor with a precisely defined geometry, converts the torque transmitted by the engine shaft into thrust, which is generated due to the pressure difference on either side of the blade [10]. Pitch, diameter, rotational speed, and blade shape are the main parameters influencing the propeller's operational efficiency and its compatibility with the engine's characteristics [7]. When designing a propulsion system for small aircraft, requirements concerning range, climb performance, ceiling, and flight endurance must be taken into account [15]. Propeller-specific coefficients, such as the thrust coefficient and power coefficient, which describe the relationship between the

power absorbed by the propeller and the thrust produced, are helpful in this regard [10].

A study concerning the AOS H2 motor glider described an instance where a propeller with a blade angle of 15°, a diameter of 0.53 m, and a rotational speed of 2300 rpm generated a static thrust of approximately 26 N [10]. The calculations were performed using a simulation method. The appropriate selection of a propeller involves achieving a trade-off between efficiency and energy consumption, whilst considering design constraints such as system mass, available engine rpm, and operating conditions [12]. In an analysis of a quadcopter, it was noted that too small a distance between the propeller disc and the fuselage leads to flow disturbances, which worsen the thrust and efficiency of the system [12]. This phenomenon was investigated using CFD simulations in ANSYS Fluent [12].

Changing the propeller itself – without any modification to the engine – affects the operating characteristics of the entire propulsion system, including the shaft's rotational speed, power requirements, and the amount of thrust generated [15]. In amateur circles, as well as in experimental aviation, tests on propellers and propulsion systems are conducted, providing a valuable source of data for academic projects and applications in general aviation [4].

Modern propellers in unmanned aerial vehicles and light aviation are most commonly made from fibre-reinforced plastics – primarily carbon fibre and nylon [16]. Research indicates that carbon fibre is characterised by greater stiffness, lower deformation, and better thermal resistance at crankshaft rotational speeds of around 6000 rpm [16]. Concurrently, nylon exhibits better resistance to impact loads, making it suitable for simpler, commercial unmanned aerial vehicles [16]. The application of various composites in aircraft, including in the construction of propulsion system components, is presented in [2]. This work lists many advantages of using such solutions: high resistance to impacts and cracking, low specific density/low mass, non-susceptibility to corrosion, low thermal expansion, non-conductivity of electricity, low relative permittivity, and vibration damping [2]. Unfortunately, these materials also have disadvantages, such as low compressive strength, difficulty in machining and processing, hygroscopicity, and high cost [2]. The use of composite materials eliminates problems associated with corrosion effects [18]. In multi-rotor aircraft such as quadcopters, the mass and stiffness of the propellers are crucial for stability, flight time, and energy consumption [5]. In most small aircraft, an important aspect is the energy consumed to generate adequate thrust, as well as flight duration or distance covered. Any additional energy loss necessitates storing more energy on board the aircraft, whether from fuel or rechargeable batteries. This, in turn, translates to an increase in the aircraft's total mass. Therefore, selecting the appropriate propeller geometry can contribute not only to increased thrust but also to an improvement in the efficiency of the entire aircraft propulsion system.

In multi-rotor aircraft such as quadcopters, the mass and stiffness of the propellers are crucial for stability, flight time, and energy consumption [5]. In most small aircraft, an important aspect is the energy consumed to generate adequate thrust, as well as flight duration or distance covered. Any additional energy loss necessitates storing more energy on board the aircraft, whether from fuel or rechargeable batteries. This, in turn, translates to an increase in the aircraft's total mass. Therefore, selecting the appropriate propeller geometry can contribute not only to increased thrust but also to an improvement in the efficiency of the entire aircraft propulsion system.

The IS-2 documentation emphasises that despite the use of a turbine propulsion system, the geometry of the tail rotor is of immense importance for performance and proper torque transfer [14]. Literature recommends verifying design assumptions through experimental measurements of torque and thrust [8]. In UAV projects, increasing emphasis is being placed on the use of advanced CAD and CAE tools for modelling propellers and optimising their shape in terms of aerodynamics [6].

Although most studies pertain to turbine engines, some conclusions are also applicable to piston-driven systems – particularly in the context of mechanical stresses in the engine-propeller assembly [1]. Monitoring operational parameters in such drive systems is becoming increasingly common, especially for early diagnostics and maintenance planning [11]. The selection and design of a propeller for a small piston engine is a task requiring a comprehensive approach. Aerodynamic and structural analysis is necessary, as is consideration of the engine's operating characteristics and the conditions under which the entire system will be operated. Modern simulation tools significantly facilitate this process, allowing for preliminary design optimisation even before physical trials commence. Materials, blade geometry, and their number are of key importance here – each of these factors directly influences the aircraft's performance. During the design phase, it is worthwhile to consider both the mechanical and thermal properties of the materials used, as well as how the propeller interacts with the rest of the structure in terms of airflow.

This research is being conducted on a 3W 275 XI B2 CS engine, which is a two-stroke engine with a displacement of 273 cm³. Although a number of publications are available on the market concerning the improvement of propeller parameters in the context of low-power engines, the majority of these works focus on theoretical analyses. Such analyses often do not correspond to real-world conditions, necessitating individual research for each specific engine. The thrust measurement results presented in this article are based on the use of a new test stand, which permits the precise and multifaceted measurement of key engine operating parameters and the thrust generated by the propeller at various angles of attack and blade profiles. The application of a load cell for thrust measurement, telemetric temperature monitoring systems, and precise rotational speed recording systems allows for the assessment of the mechanical and thermal processes occurring within the engine.

Owing to the capability for rapid exchange and adjustment of propeller blade profiles and angles of attack, this work encompasses a broad spectrum of configurations. Such a defined scope of tests allows for the identification of optimal solutions for both ultralight aircraft and unmanned

aerial vehicles of various sizes. Detailed monitoring of cylinder head temperatures, correlated with thrust data, enables the investigation of the links between propeller aerodynamics and achieved engine parameters. Consequently, it is possible to identify design and operational solutions that improve both the performance and durability of the combustion engine used. The test stand has been designed in such a way as to facilitate not only future changes to propeller shape and angle of attack but also modifications to the engine itself (e.g., testing anti-wear or thermal barrier coatings). Such versatility in shaping research conditions constitutes a significant advantage for further development work.

Thanks to these features, the presented concept combines elements of classical aerodynamic studies with advanced thermomechanical analysis of the engine. This allows for capturing the multidimensional aspect of a two-stroke aero engine's operation. There is a significant gap in research of this type utilising combustion engines. The results and methodology presented in this work can be utilised by engine and propeller manufacturers, as well as by research teams specialising in the development of modern propulsion systems for aviation applications. As such, this work makes a significant contribution to the development of engineering methods and tools for establishing methodologies for selecting propeller configurations for piston aero engines; furthermore, it fills a gap concerning practical, comprehensive analyses of the influence of propeller geometry on the operational parameters of small combustion engines.

2. Materials and methods

2.1. Construction of a test rig for propeller evaluation

The test rig was constructed to facilitate the testing of two-stroke piston engines utilised in light aviation and unmanned aerial vehicles (UAVs) (Fig. 1). Further technical details on the construction of the test stand are provided in reference [17]. The entire structure of the test rig is based on a steel frame, protected by a layer of zinc and a powder coating offering increased resistance to atmospheric conditions. The frame is equipped with four adjustable feet featuring an M16 thread, enabling precise levelling of the rig with the aid of a laser level. Mounted within the frame is a steel engine mount, adapted for the installation of two engine models: the DLE170 (a twin-cylinder, two-stroke engine with a 170 cm³ capacity) and the 3W 275 XI B2 CS (a twin-cylinder, two-stroke engine with a 273 cm³ capacity). The mount allows for the adjustment of the crankshaft axis inclination angle within a range of ±15°, which permits the engine's position to be altered relative to the force sensor [17]. Fastening is accomplished using class 12.9 bolts and spring washers, which prevent the connections from loosening during engine operation.

The supply system provides independent regulation of fuel and air flow. The fuel system comprises a 500 ml capacity tank, fuel filters, petrol-resistant silicone tubing, and a non-return valve. The fuel-oil mixture ratio is 40:1 in test mode and 30:1 during the running-in of new engine components. The oil used is Castrol Power1 A747 Racing 2T. The oil-fuel mixture can be freely selected depending on the tests being conducted and the anticipated maximum loads on the engine's main mechanical components.

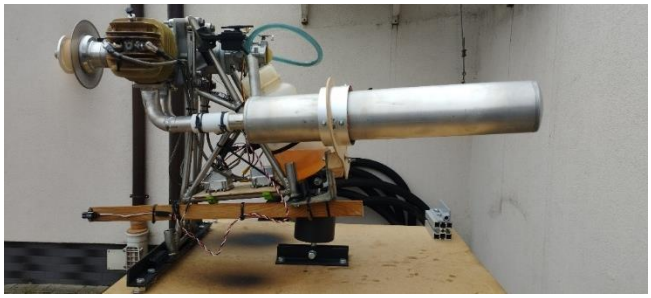

Fig. 1. Test rig construction

Cooling is provided by the thrust generated by the propeller, which is positioned close to the cylinder heads. Additionally, cooling fans can be mounted on the rig, their speed being automatically regulated according to the engine cylinder head temperature. However, for rig-based tests, it is more advantageous to conduct evaluations without utilising fans. This is because it allows for an assessment of how the thrust generated by the propeller and its geometric parameters affect the temperature change of the cylinder heads in relation to the engine crankshaft's rotational speed. The measurement system includes a CL14-type force sensor with a measurement range of up to 5 kN, a sensitivity of 1 mV/V, and linearity of ≤ 0.5%. The sensor's strain gauge bridge has an input resistance of 410 Ω and an output resistance of 350 Ω [17]. The sensor is coupled with a CL 450 data logger, enabling data recording with 24-bit resolution and a speed of up to 29,000 samples per second [17]. The recorder is equipped with an OLED screen and USB 2.0 communication capability (Fig. 2).

Fig. 2. Data logger construction

To measure the temperature, a type 1 type K-type thermocouple is used (accuracy of ± 1.5°C or 0.4% read), mounted directly in the engine block at the spark plug sockets, along with additional SBS-01T sensors.

The latter communicate via the S.BUS2 bus with a Futaba T18SZ RC transmitter and permit real-time temperature readings in the range of –20°C to +200°C (Fig. 3) [17]. Additional measurement equipment includes: an optical propeller rotational speed sensor with a resolution of 1 pulse per revolution, a Hall effect throttle position sensor, and a digital shaft rotational speed sensor integrated with the ignition

module. The engine is started using an ignition module, powered by a regulated voltage source of either 6.0 V (NiCd) or 7.4 V (LiPo) [17]. The spark plugs used are NGK CM6, and the ignition timing advance is automatically adjusted depending on the engine's operating temperature.

Fig. 3. Futaba RC Measurement and Control System

For testing purposes, the engine manufacturer recommends using propellers in various configurations: two-blade 36×12 and 36×14, as well as three-blade 32×12 and 34×12. This allows for the modelling of various dynamic load conditions on the powertrain. The rig facilitates continuous tests (up to 30 minutes of operation under steady conditions) and cyclical load changes. The collected data enable real-time analysis of engine operating parameters, including thrust, cylinder head temperatures, rotational speed, and throttle position. This facilitates the evaluation of the effectiveness of applied tribological coatings and thermal barriers on the primary mechanical components, such as the piston, piston rings, and cylinder.

2.2. Propellers utilised during rig tests

The test rig facilitates the mounting of propellers with various profiles and numbers of blades. Propeller mounting is carried out using bolts with special securing adapters. All propellers are tightened to the appropriate torque, depending on the material from which they are made (Fig. 4). The mounting assembly comprises 1 central bolt and 5 circumferentially arranged bolts. It is also important to remember that over-tightening the mounting bolts can cause excessive stress and damage to the propeller. Such an eventuality is particularly dangerous if personnel conducting measurements are located in the vicinity of the rig.

Six types of propellers were used for the rig tests. An illustrative example of mounted 2- and 3-blade propellers is shown in Fig. 5 and Fig. 6.

Fig. 4. Propeller mounting assembly

Fig. 5. 3-blade propeller made of carbon fibre

2.3. Test conditions for investigating thrust as a function of propeller geometry

To determine the weight of the individual propellers selected for testing, their weight was measured using a WLC 30/F1/K precision balance. The readability of the balance is 0.5 g, with a linearity of ±1.5 g. The balance provides readings via a display.

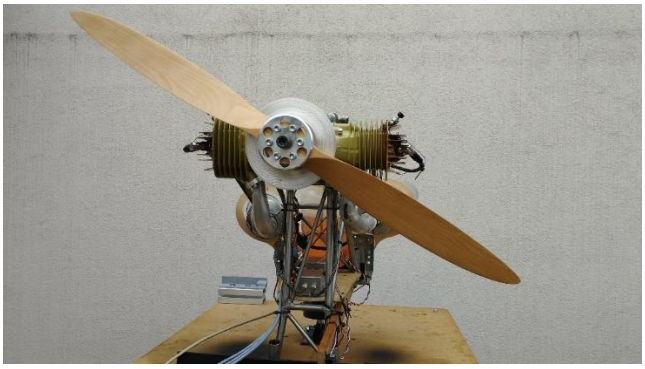

Fig. 6. 2-blade propeller made of wood

Tests utilising the test rig were conducted at an ambient temperature of approximately 10°C and a humidity of approximately 35–40%. The rotational speed range extended from idle speed to the maximum engine rotational speed. The maximum engine rotational speed is dependent on the propeller profile and geometry used. All measurements were conducted under similar ambient conditions; the influence of these conditions on the measurement results was negligible. A steady crosswind with an average speed of 16 km/h was present, and the ambient temperature during the measurements was approximately 13–14°C.

3. Results and discussion

3.1. Characteristics of propellers used in rig tests

For the rig tests, six propeller models with varying numbers of blades and dimensions were utilised.

- Fiala 2-blade propeller 30/18 (Fig. 7 and 8)
- Fiala 2-blade propeller 32/16 (Fig. 9 and 10)
- Fiala 2-blade propeller 32/18 (Fig. 11 and 12)
- Biela 3-blade propeller 32/14 (Fig. 13 and 14)
- Biela 3-blade propeller 32/12 (Fig. 15 and 16)
- Falcon 3-blade propeller 32/13 (Fig. 17 and 18).

Prior to conducting tests for thrust, cylinder head temperature, and the aero engine's crankshaft rotational speed,

preliminary measurements of the mass of all propellers were performed (Fig. 19). Readings were obtained after placing each propeller on the metal platform of the balance. This measurement provides a realistic indication of the influence of weight on the engine's operational parameters obtained, in relation to the number of blades and the propeller profile geometry. The Fiala propellers are made of wood; the Biela 32/14 propeller is constructed from a carbon and glass fibre composite using a high-strength resin. The Falcon 32/13 and Biela 32/12 propellers are made entirely of carbon fibre.

Fig. 7. Fiala 30/18 2-blade propeller – view

Fig. 8. Fiala 30/18 2-blade propeller – geometry designation

Fig. 9. Fiala 32/16 2-blade propeller – view

Fig. 10. Fiala 32/16 2-blade propeller – propeller geometry designation

Fig. 11. Fiala 32/18 2-blade propeller – view

Fig. 12. Fiala 32/18 2-blade propeller – propeller geometry designation

Fig. 13. Biela 32/14 3-blade propeller – view

Fig. 14. Biela 32/14 3-blade propeller – propeller geometry designation

Fig. 15. Biela 32/12 3-blade propeller – view

Fig. 16. Biela 32/12 3-blade propeller – propeller geometry designation

Fig. 17. Falcon 32/13 3-blade propeller – view

Fig. 18. Falcon 32/13 3-blade propeller – propeller geometry designation

3.2. Measurement of the mass of propellers used in the tests

The choice between a two-blade and a three-blade propeller is contingent upon numerous factors, such as torque requirements, crankshaft rotational speed, and the specific operational conditions of the aircraft. Differences in mass can influence the dynamic balance and energy efficiency of the entire system. There is no definitive answer as to which propeller constitutes the optimal solution for a given engine. This cannot be predicted at the assembly stage based on geometric and mass parameters. Only bench tests allow for the determination of which propeller can achieve the maximum thrust value, the thrust characteristic curve, the thermal loading on the engine heads, and the maximum attainable engine rotational speed. To a significant extent, speed and thrust determine the correct selection of the propeller profile and number of blades for a particular type of aircraft piston combustion engine. The self-mass of the propeller is influenced not only by its geometry and the number of its blades but also by the type of materials utilised. This is particularly observable in the considerably lower mass of the Falcon 32/13 propeller compared to its three-blade counterparts from Biela, models 32/12 and 32/14. The Falcon propeller is approximately 31.3% lighter than the Biela 32/14 model and about 26.5% lighter than the Biela 32/12 model. An exemplary measurement of a propeller's self-mass is depicted in Fig. 19.

A compilation of all propeller weight measurements taken during the bench tests is provided in Table 1.

Table 1. Self-mass of propellers used in the tests

Propeller name	Self-mass m [g]
Fiala 2-blade propeller 30/18	273.0
Fiala 2-blade propeller 32/16	302.0
Fiala 2-blade propeller 32/18	299.5
Biela 3-blade propeller 32/14	586.0
Biela 3-blade propeller 32/12	547.5
Falcon 3-blade propeller 32/13	402.5

Data for calculating measuring uncertainty:

- Own weight of propellers – values from Table 1: 273.0–586.0 g
- Laboratory scale WLC 30/F1/K – Read plot d = 0.5 g, linearity ±1.5 g (manufacturer specification)
- Five measurements were carried out for each propeller and the same reading on the measuring weight was obtained.

Type A uncertainty (repeatability)

$$u_a = \frac{s}{\sqrt{n}} \tag{1}$$

where: s = 0, s – standard deviation of the mass measurements series (here s = 0, s = 0 g, because all readings were identical), n – number of measurement repetitions (here n = 5).

Type B uncertainty (characteristic of the device)

Display resolution:

$$D = 0.5\ g \rightarrow u_d = \frac{d}{2\sqrt{3}} = 0.144\ g \tag{2}$$

Nonliney of the weight:

$$\pm 1.5\ g \rightarrow u_{lin} = \frac{1,5}{\sqrt{3}} = 0.866\ g \tag{3}$$

The total standard uncertainty is:

$$u_c = \sqrt{u_d^2 + u_{lin}^2} = \sqrt{0.144^2 + 0.866^2} = 0.878\ g \tag{4}$$

Extended (trust level 95 %, k = 2k = 2):

$$U = 2u_c = 1.756\ g \tag{5}$$

where: d – reading plot (readability) of weight; the mass difference corresponding to the change by one display, U – extended uncertainty, u_c – total standard uncertainty, u_d – a component of standard uncertainty caused by the completed display resolution, u_{lin} – a component of standard uncertainty associated with weight non-linearity.

The measurement-uncertainty results for the propeller masses are presented in Table 2.

Table 2. Self-mass of propellers used in the tests

Propeller Name	Self-mass [g]	Expanded uncertainty U (95%) [g]	Relative uncertainty U/m [%]
Fiala 2-blade propeller 30/18	273.0	1.756	0.643
Fiala 2-blade propeller 32/16	302.0	1.756	0.581
Fiala 2-blade propeller 32/18	299.5	1.756	0.586
Biela 3-blade propeller 32/14	586.0	1.756	0.300
Biela 3-blade propeller 32/12	547.5	1.756	0.321
Falcon 3-blade propeller 32/13	402.5	1.756	0.436

Zero deviations of the series confirm the good repetition of the weight, but does not remove the main restriction – non-linearity ±1.5 g. A relative uncertainty below 1% – even for the lightest propeller - is sufficiently small for analysing the forces and energy of the propulsion system; periodic calibration of the balance to verify its non-linearity parameter is more important than performing additional weighing.

Fig. 19. Exemplary measurement of propeller mass using WLC 30/F1/K scales – result 273.0 g

3.3. Study of the relationship between thrust, shaft rotational speed, and head temperatures

All propellers tested demonstrate a direct relationship between thrust and crankshaft rotational speed – as the rotational speed increases, so does the thrust. However, the thrust characteristics vary depending on the specific model and type of propeller. To determine the propeller-generated thrust of the propulsion system accurately, the correction coefficient k_G must be established. It depends on the distances A and B. In this case, A equals 0.4245 m and B equals 0.3329 m. This value should be verified experimentally, not just geometrically. If a different engine is installed in the frame, the coefficient k_G may change, so the corresponding geometric measurements and mass-load verification must be repeated.

In the tested dynamometer, the track power measurement is not performed in the drive axis, but on a strainometric sensor attached to the back of the frame. There is a lever system (Fig. 20) between the propeller axis and the sensor) with two arms.

From a condition of the moments for static load:

$$F_S B = F_T A \tag{6}$$

$$F_T = F_S \frac{B}{A} \rightarrow k_G = \frac{A}{B}, F_T = \frac{F_S}{k_G} \tag{7}$$

$$k_G \approx 1.27516 \tag{8}$$

where: A – distance from the axis of the propeller to the front bed (engine mounting point to the frame), B – distance from the axis of the propeller to the axis of the force sensor, F_S – the force recorded by the strain-gauge sensor mounted at the rear of the frame [N], F_T – the actual static propeller thrust along the drive axis [N], k_G – the factor calculated by the geometric method.

To accurately verify the calculated value of the correction coefficient, precise experimental measurements are performed. In such a case, a line is mounted exactly on the propeller axis, set to be perfectly parallel with the axis, the alignment of which is verified using a spirit level. At the end of the line, there is a wheel attached to a post opposite the test stand. A weight of an appropriate mass is suspended from the end of the line. In this instance, calibration of the read values was performed for masses of 10 kg and 20 kg. The value from the sensor was read and then corrected against the actual load suspended on the line. This value is accurate and serves as an additional verification of the conversion coefficient.

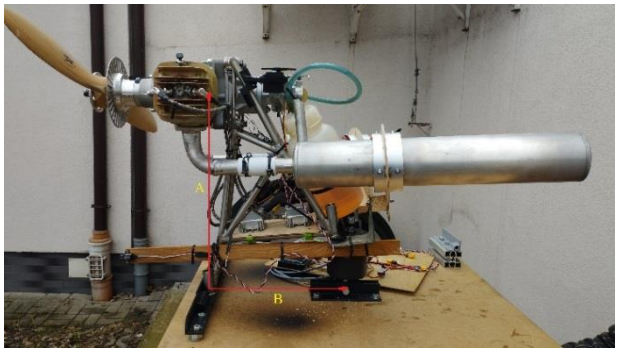

Fig. 20. Calculating the correction coefficient value

To verify the correctness of the calculated k_G, an independent calibration test with a known applied load is performed. To confirm the correctness of the calculated k_g (geometrically determined from a distance A = 0.4245 m and B = 0.3329 m → $k_G \approx 1.27516$) an independent standard examination is performed by strength load.

Verification of the parallelism of the rope from the axis is done using a 0.1° accuracy level. The verification test uses a 2 mm steel rope, with its stretchiness 0.2% for 1 kN. A block with ball bearings with an efficiency of about 0.995 was also used, which minimizes friction losses. The rope is attached concentrically to a spacer sleeve bolted in place of the propeller hub.

The wire runs parallel to the engine axis. A deviation of less than 0.5 mm over a distance of 1 meter is checked with a spirit level. A pulley is installed on the opposite post. The free end of the wire hangs vertically, 1.0 meter above the ground.

The test uses 10 kg and 20 kg M1 class weights, providing a tolerance of ±5 g. The CL14 force sensor has a nonlinearity of ≤ 0.5%. The value of g was taken as 9.80665 m/s² for Warsaw.

For a mass of 10 kg, the reference force (F_{Tw}= mg) is 98.066 N, and for a mass of 20 kg, the reference force is 196.133 N. For the 10 kg mass, the sensor output was 125.2 N, and for the 20 kg mass, the sensor output was 249.7 N.

The value of the coefficient determined experimentally using reference masses k_{exp} can be calculated from the following formula:

$$k_{exp} = \frac{F_S}{F_{Tw}} \tag{9}$$

Accordingly k_{exp} for the 10 kg mass is 1.2767, and for the 20 kg mass it is 1.2731. After calculating the mean value from the reference measurements k_{exp} = 1.2749.

The difference between the coefficients k_{exp} and k_G is:

$$k_{exp} - k_G = 0.00026\ (0.02\%) \tag{10}$$

The uncertainty calculation for determining the coefficient k includes the following components:

- Force sensor nonlinearity, limit ±0.5F, rectangular distribution, standard deviation u_i = 0.289% and relative standard deviation u_i/k = 0.00289
- Pulley friction, limit ±0.5 F, rectangular distribution, standard deviation u_i = 0.289% and relative standard deviation u_i/k = 0.00289
- Mass of the weights, limit ±5 g, rectangular distribution, standard deviation u_i = 0.029% and relative standard deviation u_i/k = 0.00029
- Acceleration due to gravity (g), limit $\pm 5\times10^{-5}$, rectangular distribution, standard deviation u_i = 0.003 % and relative standard deviation u_i/k = 0.00003
- Wire alignment (0.2°), limit ±cosθ, normal distribution, standard deviation u_i = 0.006% and relative standard deviation u_i/k = 0.00006
- Sensor thermal drift, limit ±0.05%/°C, ΔT=5°C, rectangular distribution, standard deviation u_i = 0.029% and relative standard deviation u_i/k = 0.00029. The value of

0.029% applies when the temperature changes by no more than ~1°C during a short weight test.

Accordingly, the combined standard uncertainty u_k is:

$$u_k = \sqrt{\sum u_i^2} = 0.409\% \tag{11}$$

The expanded uncertainty (95%) U_k is:

$$U_k = 2u_k = 0.82\% \tag{12}$$

The accuracy of the performed calculations—the difference of 0.02% between k_{exp} and k_G is 40 times smaller than the calculated expanded uncertainty of 0.82%. The experimental method confirms the geometric value k_G with a large margin of confidence. Therefore, it can be stated that the value 1.275, adopted for correcting the force readings from the sensor, is very accurate. The largest contributions to the uncertainty budget (45% each) come from the sensor nonlinearity and pulley friction. Improving either of these components will reduce U_k below 0.6%.

The value of U_{FS}/F_S comes from the following specification for the CL14 sensor:

- Force sensor nonlinearity, limit ±0.5 F, rectangular distribution, standard deviation $u_i/F_S = 0.289\%$
- Repeatability (noise), limit ±0.15 (1σ), normal distribution, standard deviation $u_i/F_S = 0.150\%$
- Sensor thermal drift, limit ±0.25%, rectangular distribution, standard deviation $u_i/F_S = 0.144\%$
- A/D converter resolution (24 bit, 5 kN range), limit ±0.04% $F_S \rightarrow \leq 0.02\%$ of reading, rectangular distribution, $u_i/F_S = 0.02\% / \sqrt{3} = 0.012\%$.

Total standard uncertainty of the sensor:

$$\frac{u_{FS}}{F_S} = \sqrt{\sum u_i^2} \approx 0.332\% \tag{13}$$

Expanded uncertainty (coverage factor k = 2):

$$\frac{U_{FS}}{F_S} = \frac{2u_{FS}}{F_S} \approx 0.664\% \tag{14}$$

In engineering reports, it is often assumed that the final uncertainty should be rounded up to the first significant digit. 0.664% → 0.7% is already a rounding, but increasing it to 1% provides an additional margin for potential sources that are difficult to quantify (such as frame microvibrations, humidity changes, minor power supply drifts in the bridge circuit).

Accordingly, the contribution to the total thrust uncertainty can be calculated using the following formula:

$$F_T = \frac{F_S}{k} \tag{15}$$

$$\frac{U_{FT}}{F_T} = \sqrt{\left(\frac{U_{FS}}{F_S}\right)^2 + \left(\frac{U_k}{k}\right)^2} \approx$$

$$\approx \sqrt{(1.0\%)^2 + (0.82\%)^2} \approx 1.3\% \tag{16}$$

Thus, thanks to the verification of k, the total measurement uncertainty of thrust does not exceed 1.3%, which is a very good result for this type of experimental research.

The method of verifying the coefficient and determining its value is effective and easily repeatable. It should be performed after each change in the position of the engine or sensor, as well as periodically (e.g., every 50 hours of test bench operation).

In the case of temperatures recorded by sensors, the main components of uncertainty and standard deviation are: u_{TC} – type K thermocouple tolerance, class 1, limit ± max {1.5°C; 0.4% T}, rectangular distribution, standard deviation $u_i = 0.866$°C, u_{CJC} – cold junction compensation error (CL450), tolerance ±0.5°C, rectangular distribution, standard deviation $u_i = 0.289$°C, u_{res} – display resolution, tolerance ±0.5°C, rectangular distribution, standard deviation $u_i = 0.289$°C, u_{rep} – repeatability, noise, interferences, normal distribution, standard deviation $u_i = 0.200$°C, u_{inst} – contact with the pipe (thermal paste + clamp pressure), tolerance ±2.0°C, rectangular distribution, standard deviation $u_i = 1.155$°C.

The total standard uncertainty for temperature measurement is:

$$u_c = \sqrt{u_{TC}^2 + u_{CJC}^2 + u_{res}^2 + u_{rep}^2 + u_{inst}^2} \approx$$

$$\sqrt{0.866^2 + 0.289^2 + 0.289^2 + 0.200^2 + 1.115^2}$$

$$\approx 1.514\text{°C} \tag{17}$$

Extended uncertainty (95 %, K = 2) is:

$$U = 2u_c = 3.03\text{°C} \tag{18}$$

Relative uncertainty for an example value t = 60°C

$$\frac{U}{T} = \frac{3.03}{60} \approx 5.0\% \tag{19}$$

The thermal contact of the sensors has become the dominant component affecting the uncertainty of the measurement (59% of the total balance). The accuracy can be improved using: stronger mechanical pressing of the sensor, a thinner layer of paste with a higher conductivity or increase the measurement time to stabilize the temperature for a given engine mode.

Based on the analysis of measurement data concerning three models of Fiala 2-blade propellers – 30/18, 32/16, and 32/18 – a number of significant conclusions can be drawn regarding their operating characteristics, efficiency, and impact on the engine's thermal conditions. For all propeller variants, the obtained values for thrust and temperature were approximated using a power function.

The Fiala 30/18 propeller exhibits a linear, yet moderate, increase in thrust in the low and medium crankshaft rotational speed ranges; however, at values above 5200 rpm, thrust increases more significantly. The maximum thrust value is approximately 460 N (Fig. 21). Nevertheless, this propeller achieves its best thrust parameters only above 5700 rpm. The average temperature recorded by sensors is about 50°C. It increases as the crankshaft rotational speed increases. Nonetheless, this temperature (or its increase) is slight, which is due to the short duration of the test conducted under very stable engine operating conditions. At maximum thrust, this temperature is approximately 48–49°C (Fig. 22). This indicates that maximum engine power is achieved with this propeller. A small increase in the temperature recorded by sensors can also be observed in the range from 3300 to 4600 rpm. In the case of both sensors,

the temperature remained at a similar level, depending on the crankshaft rotational speed.

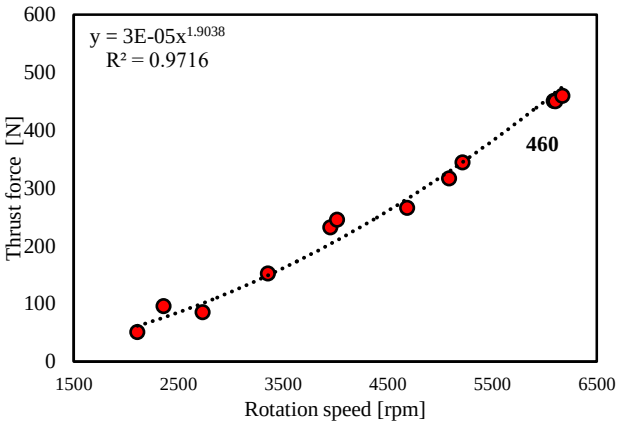

Fig. 21. Corrected thrust obtained for the Fiala 30/18 propeller as a function of crankshaft rotational speed

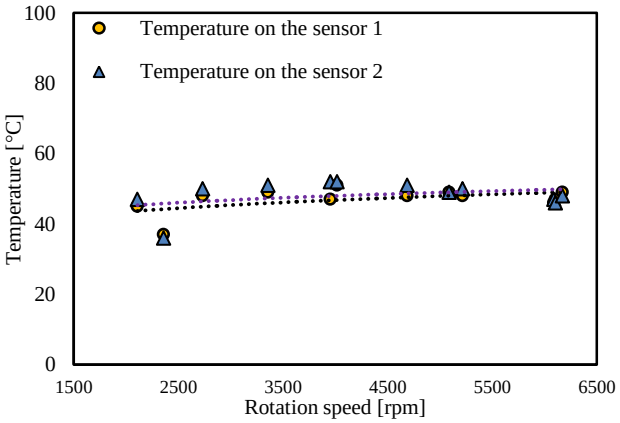

Fig. 22. Measured engine head temperature during tests of the Fiala 30/18 propeller for given engine rotational speeds.

The Fiala 32/16 model, in comparison to the previous one, achieves higher maximum thrust values – up to approximately 498 N – at a lower rotational speed (approx. 5853 rpm) (Fig. 23). This represents an increase in thrust of approximately 8.26% compared to the previous propeller. In the lower range of the crankshaft speed (up to about 3800 rpm) the engine operates at higher temperatures in part of the head, reaching about 64°C; However, as the shaft speed increases and a greater string, the temperature is recovered by the sensors – ultimately to even 41°C. This indicates that this propeller is designed for operation at high shaft rotational speeds, and its geometry allows for more effective utilisation of the engine's power output in the upper shaft rotational speed range. Higher shaft speeds with this type of propeller allow better cooling, as you can observe in Fig. 24. It shows a systematic decrease in temperature as air flow increases, resulting from the increase in speed and draft. This propeller is characterised by a gradual increase in thrust relative to the increase in shaft rotational speed. The most effective operating parameters for the power unit with this propeller are achieved in the 5500 rpm to 5850 rpm range.

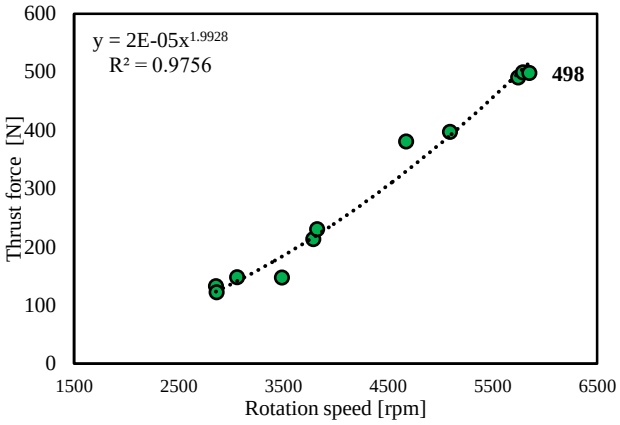

Fig. 23. Corrected thrust obtained for the Fiala 32/16 propeller as a function of crankshaft rotational speed

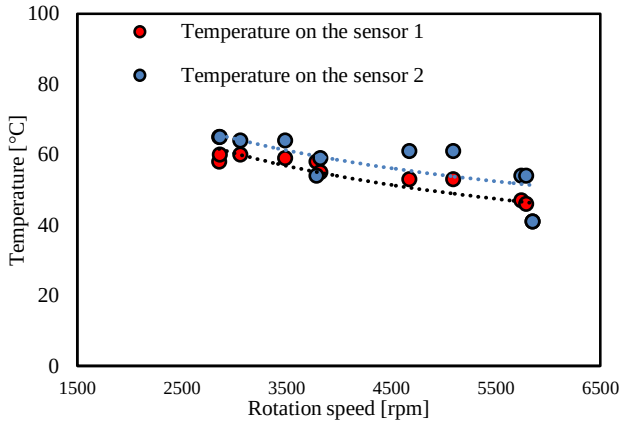

Fig. 24. Measured engine head temperature during tests of the Fiala 32/16 propeller for given engine rotational speeds.

The Fiala 32/18 propeller, in turn, is characterised by a relatively high thrust value even in the low shaft rotational speed range – for example, at just 3500 rpm, it generates approximately 200 N, which, compared to other models, makes it exceptionally effective in the low shaft speed range (Fig. 25). The temperatures recorded by the sensors are much higher, on average about 70°C, which may indicate a higher engine load compared to the previous variants of the propeller (Fig. 26). The temperature in the scope of both engine heads is the highest in the lower and upper ranges of the engine shaft speed. This is certainly related to achieving a good engine torque distribution in this range. The maximum thrust value obtained is 476 N, at a rotational speed of 5610 rpm. Based on the data, it can be observed that this propeller allows the lowest crankshaft rotational speed to be achieved. Despite this decrease in rotational speed, a high thrust value can be achieved. At maximum thrust, an increase in head temperature is visible. Nevertheless, a decrease in head temperature is noted in the 5000 rpm to 5500 rpm range. However, it should be generally assumed that the temperature remains almost constant at different rotational speeds of the engine shaft.

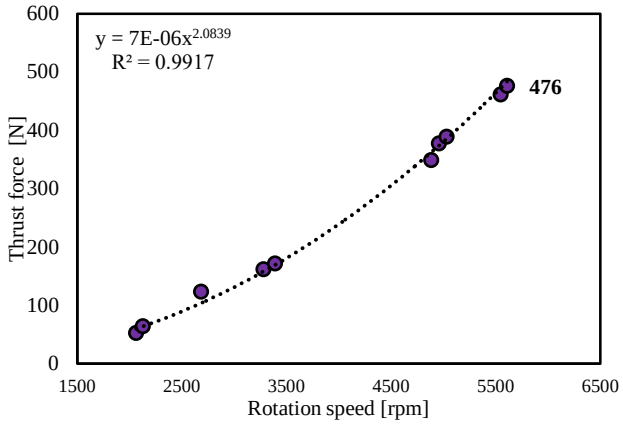

Fig. 25. Corrected thrust obtained for the Fiala 32/18 propeller as a function of crankshaft rotational speed

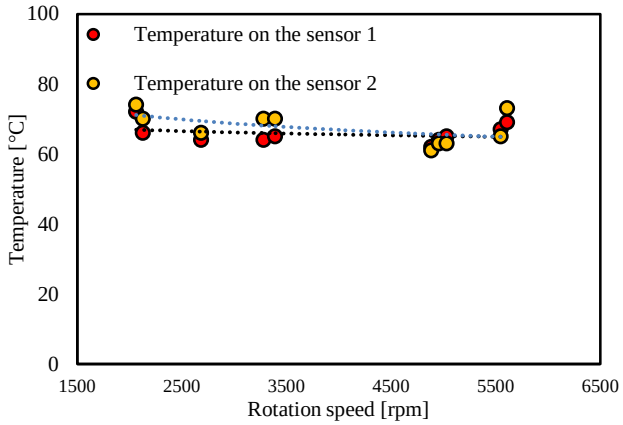

Fig. 26. Measured engine head temperature during tests of the Fiala 32/18 propeller for given engine rotational speeds

In the case of the Biela 32/14 3-blade propeller, an increase in thrust is observed in the shaft rotational speed range of 3700 rpm to 3800 rpm; whereas in the higher crankshaft speed range, this increase levels off. At a rotational speed of approximately 4936 rpm, a maximum thrust value of close to 529 N was achieved (Fig. 27). Such a thrust characteristic curve may indicate that the propeller achieves its highest aerodynamic efficiency in the mid-range of rotational speeds. The influence of shaft rotational speed on temperature distribution is significant. Figure 28 shows a decrease in temperature as the shaft speed increases, which undoubtedly promotes better cooling due to air flow. Even after reaching the maximum speed and shaft, the temperature is low, from 46 to 48°C. In this case, as the propeller's speed increases, the temperature decreases slightly, indicating better cooling than in the case of 2-blade propellers. The same applies to the generated thrust.

According to the data in Fig. 29 for the Biela 32/12 3-blade propeller, a sudden and dynamic increase in the thrust value can be observed starting from a shaft rotational speed of approximately 4000 rpm. With this propeller, relatively high thrust values can be obtained at a reduced shaft rotational speed in the range of 4484 to 5392 rpm. In this case, the temperature is stable in the entire range of shaft speed, between 55 and 60°C (Fig. 30). At the average speed of the shaft, a small decrease in the temperature recorded by the sensors can be observed. This is due to a lower engine load and improved airflow in this rotational speed range, as a result of its thrust characteristics. This propeller generates a maximum thrust of 524 N, which is a similar value to that of the previous 3-blade propeller variant. However, in this instance, this thrust is achieved only in the higher shaft rotational speed range. In this case, an increase in the maximum shaft rotational speed of over 400 rpm can also be observed. This indicates that this propeller imposes a lower load on the engine.

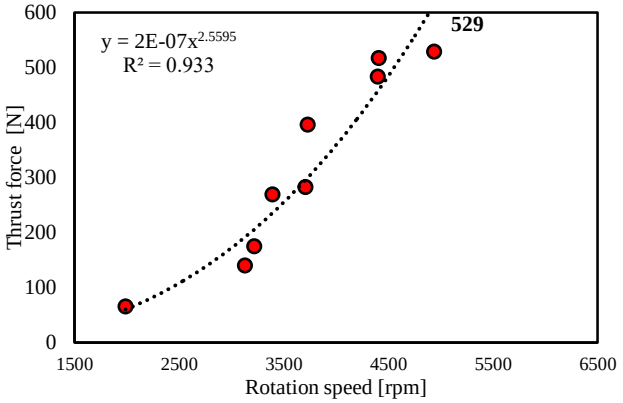

Fig. 27. Corrected thrust obtained for the Biela 32/14 propeller as a function of crankshaft rotational speed

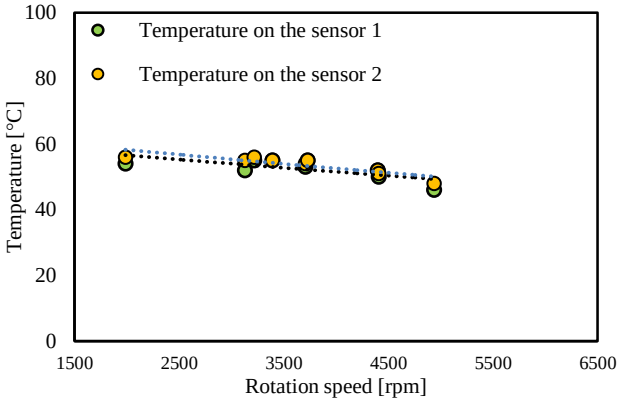

Fig. 28. Measured engine head temperature during tests of the Biela 32/14 propeller for given engine rotational speeds

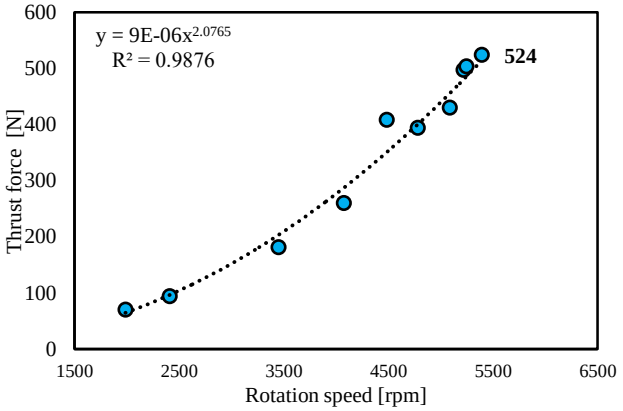

Fig. 29. Corrected thrust obtained for the Biela 32/12 propeller as a function of crankshaft rotational speed

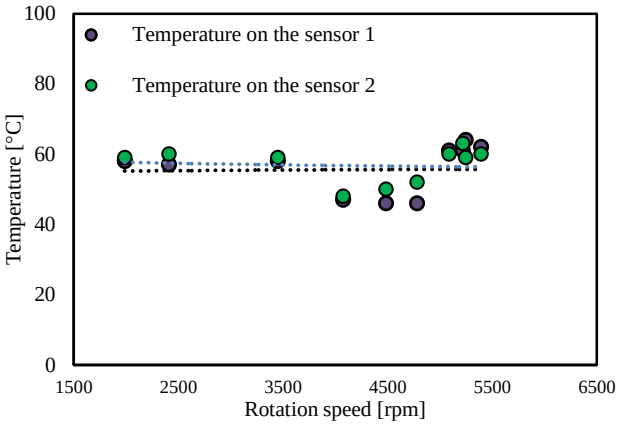

Fig. 30. Measured engine head temperature during tests of the Biela 32/12 propeller for given engine rotational speeds

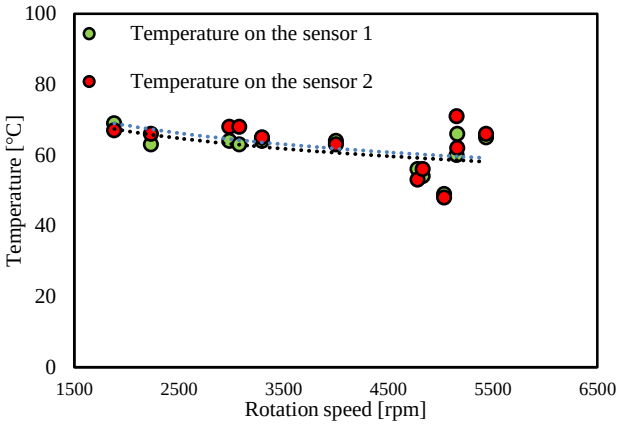

Fig. 32. Measured engine head temperature during tests of the Falcon 32/13 propeller for given engine rotational speeds

According to the results in Fig. 31, the Falcon 32/13 propeller generates the highest thrust of all the variants. The maximum thrust recorded is 569 N at 5162 rpm. According to its thrust characteristic, a linear progression of thrust with respect to shaft rotational speed can be observed. At higher shaft rotational speeds, the thrust decreases slightly. The progression of the obtained thrust is very stable from a speed of approximately 4700 rpm onwards, as can be observed in Fig. 31. This propeller also enables good cooling of the engine heads. The average temperature in the entire speed of the shaft speed is about 62°C, with the temperature decreasing as the thrust increases. It can be considered that this propeller is the best variant overall. Additionally, its relatively low self-mass for a 3-blade category propeller indicates a low load on the engine. This (its low mass) is well-balanced with the achieved thrust and the engine's operating temperature.

The lightest wooden biplane propellers by Fiala (273–302 g) generate thrust ranging from 460 N (model 30/18) to 498 N (32/16) at very high shaft rotational speeds – specifically, 6171 rpm and 5853 rpm, respectively. Their efficiency index T/m exceeds 1600 N kg^{-1}, which makes them unrivaled when the thrust-to-mass ratio is the key criterion. Unfortunately, this is associated with drawbacks such as higher noise levels and increased fuel consumption resulting from the high shaft speeds.

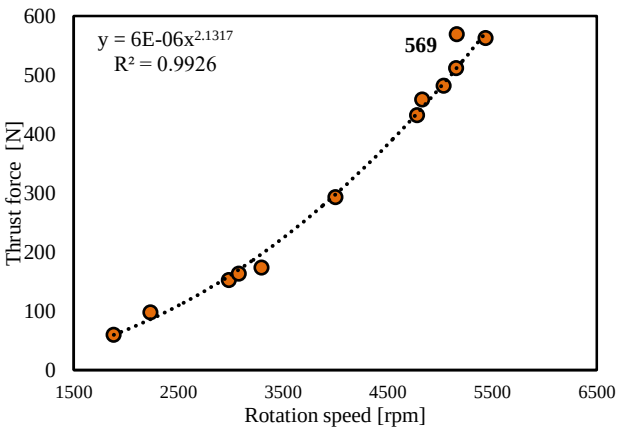

Fig. 31. Corrected thrust obtained for the Falcon 32/13 propeller as a function of crankshaft rotational speed

The Falcon 32/13 three-blade propeller, made entirely of carbon fiber, weighs 402 g about one third less than the composite Biela 32/14 propeller and one quarter less than the Biela 32/12. Thanks to the high stiffness of carbon fiber, the Falcon 32/13 propeller achieves the highest thrust value (569 N) already at moderate rotational speeds of 5162 rpm, maintaining an efficiency index T/m of 1414 N kg^{-1}. In comparison, the composite propellers from Biela are heavier (547–586 g), and their maximum thrust (524–529 N) is developed at even lower shaft speeds of 4936–5392 rpm. In this case, however, the higher mass reduces their efficiency to 903–958 N kg^{-1}. The advantage of the thicker carbon-glass laminate in the Biela 32/14 is the best cylinder head cooling – the lower rpm and greater inertia of the airflow reduce cylinder temperatures by about 8°C compared to the wooden Fiala propellers.

The data comparison clearly shows that mass determines the specific efficiency (T/m), while the material and blade stiffness dictate the required shaft rotational speeds and the engine's thermal load. Wooden propellers are an excellent choice when minimum weight is essential and high shaft speeds are acceptable. The Falcon carbon fiber propeller offers the best compromise between maximum thrust, mass, and a moderate rpm range. The heavier Biela composite propellers are recommended when reducing noise and cylinder head temperatures is the priority, even at the expense of a lower T/m index. The quantitative comparison introduced here fills a gap by demonstrating a clear relationship between geometry, material, mass, and the actual performance of each tested propeller.

The diameter of the Falcon propeller is 0.813 m, so the disk area is 0.519 m². Using the momentum equation:

$$v = \sqrt{\frac{T}{2\rho A}} \tag{20}$$

At ρ = 1.2 kg m^{-3}, the jet velocity is 21.4 m s^{-1}. The ideal power $P_i = \frac{1}{2}Tv$ is 6.1 kW. With typical data for three-blade propellers of this size – static efficiency 0.55 ±0.05 – the required shaft power is 11.1 ±1.0 kW. According to the manufacturer, the 3W 275 XI engine delivers 20–22 kW at 7000 rpm; therefore, at the rotational speed of 5162 rpm corresponding to a thrust of 569 N, there remains a 45% power reserve.

A number of factors explain why the Fiala 30/18 propeller requires as much as 6171 rpm, while the Biela 32/14 propeller needs only 4936 rpm. This is mainly related to the number of blades: each additional blade increases induced and mass drag, so the three-blade Falcon and Biela propellers reach their target thrust at around 5100 rpm, whereas the lighter two-blade Fiala propellers require higher rotational speeds to generate the same thrust. The total pitch also influences these parameters. The Biela 32/14 has a pitch of 14″, greater than the 13″ of the Falcon and the 12″ of the Biela 32/12; therefore, at the same engine torque, its shaft speed is significantly lower. Another factor is material stiffness. The wooden blades of the Fiala propellers flex under heavy load, reducing the angle of attack, which necessitates higher shaft speeds, while the Falcon carbon fiber propeller maintains its angle at lower shaft speeds. Another significant factor is inertia. The heaviest propeller, the Biela 32/14 (586 g), exhibits the highest moment of inertia, which stabilizes the shaft rotational speed at a lower level.

3.4. Limitations of the test stand and research methodology

The test stand has certain limitations concerning the results obtained, which must always be precisely defined during various tests. These primarily stem from the engine's thermal inertia during tests and changes in external conditions. Rapid changes in the temperature of the heads and the main engine mechanism after conducting a test run make it difficult to maintain stable measurement conditions. Establishing initial test conditions, namely temperature and humidity, is essential for drawing correct conclusions. Another limitation is the very movement of the frame's moving parts along with the engine. As a result of small clearances, this error is relatively minor, but it exists, and attention must always be paid to these initial test conditions. Therefore, it is always worthwhile to perform an experimental verification of the correction coefficient for each engine mounted. The measurement error is also significantly influenced by the head temperature, which constitutes a thermal load on the main mechanism. However, in this instance, the propeller profile and airflow determine the temperature achieved. Consequently, thrust results should always be checked against head temperatures, and conclusions subsequently drawn.

4. Conclusion

The research carried out confirmed that the angle of attack and profile of the blades, as well as the number of propeller blades, have a significant impact on the performance parameters achieved by the 3W 275 XI B2 CS two-stroke aero engine. Changes in propeller geometry translate directly into the thrust generated, crankshaft rotational speed, and also the engine's thermal conditions. It was also observed that the mass and structural rigidity of the propeller can determine the operational dynamics of the power unit throughout its full rotational speed range.

– The highest thrust value (569 N) was recorded using the Falcon 32/13 3-blade propeller (with a mass of 402.5 g), simultaneously achieving a shaft rotational speed of approximately 5436 rpm. This indicates the high aerodynamic efficiency of this variant and favourable head cooling conditions in the higher shaft rotational speed range of the piston aero engine.
– The 2-blade propellers (Fiala 30/18, 32/16, 32/18) achieved maximum thrust values ranging from 460 N to 498 N, depending on configuration and rotational speed (up to approx. 6000 rpm). Conversely, the 3-blade propellers (Biela 32/12, 32/14, Falcon 32/13) achieved higher thrust values – even exceeding 569 N – but in some cases, this required greater drive torque and resulted in an unfavourable temperature distribution.
– The greatest thermal load on the engine was observed during the initial phase of operation with the Fiala 32/18 propeller at medium rotational speeds (3000–4000 rpm), when the engine had to overcome significant aerodynamic drag from the propeller with an insufficiently strong cooling airflow.
– The mass of individual propellers ranged from 273 g (Fiala 30/18) to 586 g (Biela 32/14), representing a difference of as much as 30%–40% between individual 3-blade models. Self-mass primarily affects the system's inertia and the dynamic loads on the engine. Lighter propellers (e.g., Falcon 32/13) enabled faster attainment of higher shaft rotational speeds and thrust values with relatively low engine head temperatures.
– The tests demonstrated that there is no universal propeller that provides maximum thrust with simultaneously low thermal load for every small piston combustion engine. The selection of propeller configuration (profile, angle of attack, number of blades) must be verified each time through bench tests. Differences in rotational speed (even 300–500 rpm) or propeller mass (even 200 g) can determine the operational efficiency of the entire power unit and engine durability.

The presented results indicate that engine bench tests with varying propeller configurations enable the identification of a compromise between the thrust obtained, thermal load, and the engine shaft's rotational speed characteristics. This allows the power unit parameters to be appropriately adapted to operational assumptions – e.g., for aircraft flights at high speeds and the potential to achieve a higher aircraft operational ceiling. In the long term, the results of this research are significant for the safety and reliability of light aircraft, particularly in the context of extending engine service life through correct cooling conditions and optimal operation within selected shaft rotational speed ranges. An appropriately selected and relatively high thrust achieved by the power unit, and its appropriate distribution relative to shaft rotational speeds, allows for high flight dynamics. This is particularly important in combat or aerobatic flights of small aircraft. It should be remembered that the results for maximum thrust and temperature values may vary slightly between individual tests; this is mainly related to the test execution procedure. This primarily concerns the timing of the measurement: whether it is taken after the engine has warmed up or during its initial operational phase. Therefore, measurements should always be carried out under the same conditions for each propeller variant.

Acknowledgements

The paper was elaborated based on data obtained during the research carried out as part of the following project: A multi-sensor platform for imaging and detecting threats occurring in areas with high dynamics of changes in environmental conditions – DOB-SZAFIR/01/ B/038/04/2021 – funded by the National Centre for Research and Development, which was implemented at the Military University of Technology. Special thanks go to the staff of the Laboratory of Air Professions, Mr J. Milczarczyk, Mr D. Czekaj, and Mr D. Borcuch, for their technical support.

Bibliography

[1] Balicki W. Potrzeby i sposoby diagnozowania lotniczych silników turbinowych (in Polish). Prace Instytutu Lotnictwa. 2009;4(199):109-116. https://yadda.icm.edu.pl/baztech/element/bwmeta1.element.baztech-article-BSW4-0089-0014/c/Balicki_potrzeby_PIL_199_2009.pdf

[2] Błachnio J, Chalimoniuk M, Nidzgorska A. Selected applications of composites in the military. J Konbin. 2023;53(4):191-210. https://doi.org/10.5604/01.3001.0054.1761

[3] Bonisławski A, Juchniewicz M, Piotrowski R. Projekt techniczny i budowa platformy latającej typu quadrocopter (in Polish). Pomiary Automatyka Robotyka. 2014;91-97.

[4] Dunna MH, Tinetti AF, Nark DM. Open rotor noise prediction using the time-domain formulations of Farassat. Aeroacoustics. 2015;14(1-2);51-86.

[5] El-Sayed AF. Piston engines and propellers. El-Sayed AF, (ed.). Fundamentals of aircraft and rocket propulsion. Springer. London 2016. https://doi.org/10.1007/978-1-4471-6796-9_4

[6] Federal Aviation Administration. Helicopter flying handbook. Chapter 4. Washington (DC): U.S. Department of Transportation; 2023. Available from: https://www.faa.gov/sites/faa.gov/files/regulations_policies/handbooks_manuals/aviation/helicopter_flying_handbook/hfh_ch04.pdf

[7] Garner WB. Model airplane propellers. Air-Propeller Research 2009.

[8] Gosiewski Z, Ołdziej D, Słowik M. Identyfikacja modelu dynamicznego napędu dla śmigłowca czterowirnikowego (in Polish). Prace Instytutu Lotnictwa. 2009;7(202):36-50. https://yadda.icm.edu.pl/baztech/element/bwmeta1.element.baztech-article-BSW4-0092-0005/c/Gosiewski_identyfikacja_PIL_202_2009.pdf

[9] Kachel S, Okoń T, Frant M, Majcher M. Project for a reconnaissance unmanned aerial vehicle. J Konbin. 2022;52(3):187-200. https://doi.org/10.2478/jok-2022-0032

[10] Kuźniar M. Wielokryterialna ocena doboru napędów lotniczych nowej generacji z wykorzystaniem metod energetycznych [doctoral dissertation]. Rzeszów University of Technology. Rzeszow 2020.

[11] Miloudi M, Medles K, Tilmatine A, Brahami M, Dascalescu L. Modeling and optimization of a propeller-type tribocharger for granular materials. J Electrostat. 2011;69(6).

[12] Pawełczyk M, Bibik P. Wykorzystanie nowoczesnych narzędzi inżynierskich w projektowaniu bezzałogowego wiropłata czterowirnikowego (in Polish). Prace Instytutu Lotnictwa. 2013;3-4(230-231):103-110.

[13] Piłat M, Kaznowska A. Wielopłatowe, bezprzegubowe śmigło ogonowe do śmigłowca klasy lekkiej (in Polish). Prace Instytutu Lotnictwa. 2009;201:111-120.

[14] Roman K. Śmigłowcowe eksperymentalne – latające laboratoria na bazie śmigłowca IS-2 (in Polish). Prace Instytutu Lotnictwa. 2008;3-4:194-195.

[15] Sabak R. Zespoły napędowe bezzałogowych statków powietrznych (in Polish). Prace Instytutu Lotnictwa. 2011;213:185-188.

[16] Tiruvenkadam N, Shankar SG, Kumar PM, Gowtham S. Investigation of structural and thermal analysis of drone propeller materials. J Phys Conf Ser. 2024;2925(1):012002. https://doi.org/10.1088/1742-6596/2925/1/012002

[17] Wróblewski P, Bratkowski P, Borcuch D, Kiszkowiak Ł. Prototype test stand for an aircraft piston engine for testing propeller profiles and advanced materials. Combustion Engines. 2025;201(2):165-175. https://doi.org/10.19206/CE-204319

[18] Żmudziński Z. Kompozyty i inne materiały stosowane w konstrukcjach lotniczych (in Polish). Sprawozdanie ITWL 5134/50. Instytut Techniczny Wojsk Lotniczych. Warsaw 2009.

Prof. Piotr Wróblewski, DSc., DEng. – Faculty of Engineering, University of Technology and Economics H. Chodkowska in Warsaw; Faculty of Mechatronics, Armament and Aerospace, Military University of Technology, Poland.
e-mail: *piotr.wroblewski@uth.edu.pl*

Przemysław Bratkowski, MSc., Eng. – Faculty of Engineering, University of Technology and Economics H. Chodkowska in Warsaw; Faculty of Mechatronics, Armament and Aerospace, Military University of Technology, Poland.
e-mail: *przemyslaw.bratkowski@uth.edu.pl*

Prof. Stanisław Kachel, DSc., DEng. – Faculty of Mechatronics, Armament and Aerospace, Military University of Technology, Poland.
e-mail: *stanislaw.kachel@wat.edu.pl*